Nonlinear robust approaches to study stability and post-critical behaviour of an aeroelastic plant

Andrea Iannelli, Andrés Marcos, *Member, CSS,* and Mark Lowenberg

***Abstract*—Two approaches to tackle the nonlinear robust stability problem of an aerospace system are compared. The first employs a combination of the Describing Function method and μ analysis, while the second makes use of Integral Quadratic Constraints. The model analyzed consists of an open-loop wing's airfoil subject to freeplay and LTI parametric uncertainties. The key steps entailed by the application of the two methodologies and their main features are critically discussed. Emphasis is put on the available insight on the nonlinear post-critical behaviour known as Limit Cycle Oscillation. It is proposed a strategy to apply IQCs, typically used to find absolute stability certificates, in this scenario, based on a restricted sector bound condition for the nonlinearity. Another contribution of the study is to understand how the conservatism usually associated with the IQCs multipliers selection can be overcome by using information coming from the first approach. Nonlinear time-domain simulations showcase the prowess of these approaches in estimating qualitative trends and quantitative response's features.**

***Index Terms*—Robust stability, nonlinear uncertain systems, integral quadratic constraints (IQCs), describing functions (DF).**

I. Introduction

In the last two decades great effort has been devoted in the control community to develop methodologies able to handle uncertainties and nonlinearities in a unified framework. One of the main results of this effort is represented by Integral Quadratic Constraints (IQCs) [1], a powerful tool to assess the robust stability and performance of nonlinear systems. The focal idea is to recast the system as a feedback interconnection of a Linear Time Invariant (LTI) plant G with an operator Δ that gathers nonlinearities and uncertainties, and then describe the latter in terms of constraints on its input and output channels by means of so-called multipliers. IQC can in fact be viewed as a comprehensive framework reconciling small gain techniques [2] for the study of uncertain systems on the one side, and positivity/passivity techniques for nonlinearities (Lur'e problem) on the other [3].

It is possible to deal with the study of the nonlinear robust problem within a less general framework than IQC by tackling the uncertainties and nonlinearities of the system by means of distinct tools for each. When the focus is only on LTI parameters or dynamic uncertainties, a well-established technique, which specializes the small gain theorem to the case of a structured Δ, is the structured singular value (s.s.v.) or μ analysis [2], [4]. Once the problem is recast in a Linear Fractional Transformation (LFT) fashion, a worst-case stability and performance analysis of the system can be pursued. And when the focus is the nonlinearities, a way to introduce them in the frequency domain framework is represented by the Describing Function (DF) method [5]. This technique allows, once the input signal form is specified, to substitute the nonlinear operator with a quasi-linear one whose output is a function of some input signal features.

The combination of μ and DF was originally presented in [6] and then furthered by [7]. While in these foundational works the theoretical bases of this unified approach were established, this paper gives novel interpretations of the results available within the framework, and proposes a methodology to obtain them in a systematic way. Although in this work its application to the design of aerospace systems is proposed, the approach is general and applicable to other engineering fields where is relevant the study of the post-critical behaviour of the plant.

A modern trend in the aeronautical industry is to design lightweight aircraft configurations to reduce fuel consumption and operating costs. Among the most dangerous phenomena exacerbated by wing flexibility we find flutter, a self-excited instability in which aerodynamic forces acting on a flexible body couple with its natural structural vibration modes. This problem is traditionally tackled in industry with linear nominal techniques [8], assessing the stability of the system by looking at the eigenvalues of the system.

However, the increase in flexibility and the demand for a more realistic description of the system, compel to consider cases where these hypotheses no longer hold. The aerospace industry, for example, has recently shown interest in research aimed at evaluating the effect of the uncertainties on instabilities prompted by the control surface freeplay [9], [10]. Among the practical goals of these studies, primary is the detection and characterization of Limit Cycle Oscillations (LCOs) [11]. In fact, the presence of nonlinearities leads to limited amplitude flutter, whose investigation is of well-ascertained interest in order to accomplish a satisfactory design [12]. A well-known case of an LCO problem is that of the Tornado aircraft that required redesign of its Spin Prevention and Incidence Limiting System (SPILS) due to large amplitude rate-limited oscillations [13].

The contribution of this work is twofold. On the one hand, it shows how the considered techniques can provide invaluable insight on the post-critical behaviour of nonlinear systems affected by uncertainties. The IQC framework, commonly employed to study the conditions leading to the loss of absolute stability, is applied to this scenario by adopting a restricted sector bound condition for the nonlinearity. DF method has been employed for the prediction of LCOs in

This work has received funding from the Horizon 2020 research and innovation programme under grant agreement No 636307, project FLEXOP.

A. Iannelli, A. Marcos and M. Lowenberg are with the Department of Aerospace Engineering, University of Bristol, BS8 1TR, United Kingdom. E-mail: andrea.iannelli/andres.marcos/m.lowenberg@bristol.ac.uk.

aeroservoelastic problems [14], [15], with the latter showing its application, in conjunction with μ analysis, to a plant affected by uncertainties, but no detailed study of the effect of the uncertainties in terms of nonlinear response was provided. This work presents a methodology to quantitatively assess the nonlinear robust aeroelastic behaviour by introducing the concept of worst-case LCO curve, which allows the highest level of oscillations exhibited by the system in the face of perturbations in the values of the parameters to be estimated. On the other hand, the article systematically discusses the modeling and analysis steps needed to pursue a fruitful application of these algorithms. The LFT paradigm allows the formulation of a common starting point for both approaches, and to provide a model for the plant in an efficient way (in terms of size of Δ) and reconciling sophisticated representation techniques [16] with physical understanding. The rationale underpinning each technique for the representation of parametric uncertainties and freeplay nonlinearity will be discussed, prior to verifying their effects on the results. In the IQC approach, conservatism of the analyses due to the multipliers' selection is investigated and some heuristics are discussed in view of its acknowledged effect on the accuracy of the results [17]–[19]. Preliminary results of the studies discussed in this work were presented in [20].

The layout of the article is as follows. Section II presents the theoretical problem and introduces the fundamentals of the tools. Section III describes the aeroelastic system considered in the work and show in detail how uncertainties and nonlinearities are modelled in the adopted frameworks. Section IV is dedicated to the discussion of the results obtained via DF-μ approach, whereas Section V reports on the IQC analyses. Section VI finally proposes a validation of the obtained results via nonlinear time-domain simulations.

II. Theoretical Background

This Section presents the theoretical background. Common notation is adopted [1], [2].

The goal of the work is to study the feedback interconnection shown in Fig. 1, where G is an LTI system and $\Delta : \mathcal{L}^n_{2e}[0,\infty] \rightarrow \mathcal{L}^m_{2e}[0,\infty]$ is a causal and bounded operator. The interconnection of G and Δ is *well-posed* if for each $r \in \mathcal{L}^m_{2e}[0,\infty]$ and $f \in \mathcal{L}^n_{2e}[0,\infty]$ (exogenous inputs) there exist unique $\bar{w} \in \mathcal{L}^m_{2e}[0,\infty]$ and $v \in \mathcal{L}^n_{2e}[0,\infty]$ such that the mapping from (r,f) to $(\bar{w},v)$ is causal. This is equivalent to require that $(I - G\Delta)$ is causally invertible. The interconnection of G and Δ is *absolute stable* if it is well-posed and if the mapping from (r,f) to $(\bar{w},v)$ has finite $\mathcal{L}_2$ gain.This work will investigate the stability of the interconnection, and its post-critical behaviour when Δ holds nonlinearities.

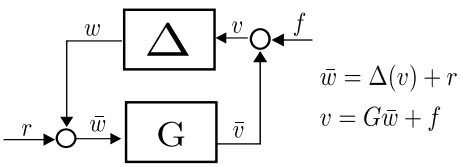

Fig. 1. Feedback interconnection.

A. LFT modeling and μ analysis

The LFT framework [2] provides a formal description of the feedback interconnection depicted in Fig. 1. Let $M \in \mathbb{C}^{(n+p)\times(m+q)}$ be partitioned as $M = [M_{11}\ M_{12};\ M_{21}\ M_{22}]$ and $\Delta \in \mathbb{C}^{m\times n}$. The upper LFT [2] with respect to Δ is:

$$\mathcal{F}_u(M,\Delta) = M_{22} + M_{21}\Delta(I - M_{11}\Delta)^{-1}M_{12} \qquad (1)$$

A crucial feature apparent in (1) is that the LFT is well posed if and only if the inverse of $(I - M_{11}\Delta)$ exists. If the operator Δ contains structured LTI uncertainties (we will indicate this by writing $\Delta = \Delta_u$), a robust stability (RS) certificate can then be obtained applying μ analysis.

The structured singular value [4] $\mu_{\Delta_u}(M_{11})$ of the complex-valued matrix M_{11} with respect to the set Δ_u is:

$$\mu = \left(\min_{\Delta_u} (\kappa : \det(I - \kappa M_{11}\Delta_u) = 0; \bar{\sigma}(\Delta_u) \leq 1 \right)^{-1} \qquad (2)$$

where κ is a real positive scalar. The result can then be interpreted as follows: if $\mu_{\Delta_u}(M_{11}) \leq 1$ then there is no perturbation matrix inside the allowable set Δ_u such that the determinant condition is satisfied, that is, the associated plant is robustly stable. On the contrary, if $\mu_{\Delta_u}(M_{11}) \geq 1$ a candidate (i.e. belonging to the allowed set) perturbation matrix exists which violates the well-posedness. $\mu_{\Delta}(M)$ is in general an NP-hard problem, thus all μ algorithms work by searching for upper bounds μ_{UB} and lower bounds μ_{LB} [4].

B. Describing Function

The Describing Function method [5] aims to provide an analogous concept of frequency response for nonlinear systems. This is pursued by means of a quasi-linearization of the nonlinear operator ϕ, after the input signal form has been specified. In this work we focus on sinusoidal-input describing functions (SIDF), later abbreviated DF. The interest in periodic signals is mainly dictated by the presence of steady oscillations in nonlinear systems, also known as LCOs [11], which are defined as isolated periodic orbits occurring in unforced dissipative systems.

The *key* hypothesis of the DF method is that only the fundamental harmonic component has to be retained from the generical periodic output at the nonlinearity. This approximation relies on the assumption that the linear element filters out the higher harmonics (*filter hypothesis*). The DF of a nonlinear element with output w is the complex fundamental harmonic gain $N(B,\omega)$ of a nonlinearity in the presence of a driving sinusoid v of amplitude B and frequency ω:

$$\begin{aligned} &N(B,\omega) = \frac{De^{j(\omega t+\theta)}}{Be^{j(\omega t)}} = \frac{D}{B}e^{j\theta} = \frac{b_1 + ja_1}{B} \\ &\text{with} \quad D(B,\omega) = \sqrt{a_1^2 + b_1^2}; \quad \theta(B,\omega) = \arctan(\frac{a_1}{b_1}) \\ &v = B\sin(\omega t); \quad w \backsimeq a_1(B,\omega)\cos(\omega t) + b_1(B,\omega)\sin(\omega t) \end{aligned} \qquad (3)$$

where a_1 and b_1 are the Fourier coefficients of the first harmonic of w. This method treats the nonlinear operator of Fig. 1 ($\Delta = \phi$ when it only gathers nonlinearities) in the presence of sinusoid inputs as if it were a linear element with a frequency response $N(B,\omega)$. Linear theory is then applied to the quasi-linearized system, searching for points of neutral stability interpreted as LCOs in the nonlinear system.

C. Integral Quadratic Constraints

IQC is a well established technique to deal with stability and performance analysis of nonlinear and uncertain systems [1] in a unified framework. Let $\Pi : j\mathbb{R} \rightarrow \mathbb{C}^{(n+m)\times(n+m)}$ be a measurable Hermitian-valued function, named multiplier. Two signals $v \in \mathcal{L}_2^n[0,\infty]$ and $w \in \mathcal{L}_2^m[0,\infty]$ (with Fourier transforms $\hat{v}$ and $\hat{w}$) satisfy the IQC defined by Π if:

$$\int_{-\infty}^{+\infty} \begin{bmatrix} \hat{v}(j\omega) \\ \hat{w}(j\omega) \end{bmatrix}^* \Pi(j\omega) \begin{bmatrix} \hat{v}(j\omega) \\ \hat{w}(j\omega) \end{bmatrix} d\omega \geq 0 \qquad (4)$$

A bounded and causal operator Δ is said to satisfy the IQC defined by Π if the signals v and $w = \Delta(v)$ satisfy (4) for all v. The next theorem [1] provides a condition for the absolute stability of the interconnection of G and Δ.

Theorem 1: Let $G \in \mathbb{RH}_\infty$ and Δ be a causal bounded operator. Assume for all $\tau \in [0,1]$:

1) the interconnection of G and $\tau\Delta$ is well-posed.
2) $\tau\Delta$ satisfies the IQC defined by Π.
3) $\exists\ \epsilon$ such that

$$\begin{bmatrix} G(j\omega) \\ I \end{bmatrix}^* \Pi(j\omega) \begin{bmatrix} G(j\omega) \\ I \end{bmatrix} d\omega \leq -\epsilon I \quad \forall\omega \in \mathbb{R} \qquad (5)$$

Then the feedback interconnection of G and Δ is stable.
In order to facilitate the numerical solution of this problem, it is common practice to factorize a multiplier Π as $\Psi^\sim\ S\ \Psi$ where $S = S^T$ is a real matrix variable and Ψ is a transfer matrix constructed from pre-selected basis transfer functions. The search for stability certificates can then be recast via KYP Lemma [1], [17] into a Linear Matrix Inequality (LMI) problem. In particular, stability is guaranteed if there exists a matrix $P = P^T$ such that:

$$\begin{bmatrix} \check{A}^T P + P\check{A} & P\check{B} \\ \check{B}^T P & 0 \end{bmatrix} + \begin{bmatrix} \check{C}^T \\ \check{D}^T \end{bmatrix} S \begin{bmatrix} \check{C} & \check{D} \end{bmatrix} < 0 \qquad (6)$$

with $[\check{A},\ \check{B},\ \check{C},\ \check{D}]$ obtained from the state-space realizations of G and Ψ. This represents the standard way to solve IQC problems, and IQCβ toolbox [21] will be employed here.
The core effort is then to find suitable multipliers Π_i describing the input/output relation of the operator Δ, since most of the conservatism associated with the results is related to this.

III. Problem statement

In the past two decades it has been clearly asserted the need to take into account the effects of uncertainties [22] and nonlinearities [12] when studying aeroelastic phenomena. In particular, LCOs, introduced in Section II-B, must be avoided in mechanical systems since they are likely to degrade fatigue life and provoke critical damages. Aircraft design requirements formulate constraints on LCO accelerations in prescribed points of the airframe [9]. These quantities can be estimated provided that a characterization of the LCO in terms of *amplitude* and *frequency* is available, hence motivating the focus of this work.

The considered test case is the benchmark study of an airfoil affected by control surface (or flap) freeplay, which has been investigated by means of different approaches: experimental [23], analytical [24], harmonic-balance method [25], continuation methods [14] and DF-μ analysis [15]. These works contributed to characterize the nonlinear flutter behaviour of the test bed, with only the last one including the effects of uncertainties in the model. In this Section the modeling steps required for the analyses are discussed.

A. Aeroelastic model

The system is shown in Fig. 2. It consists of a rigid airfoil with lumped springs simulating the 3 degrees of freedom (DOFs): plunge h, pitch α and trailing edge flap β. The position of elastic axis (EA), center of gravity (CG) and aerodynamic center (AC) is marked in Fig. 2. The parameters in the model are: K_h, K_α and K_β –respectively the bending, torsional and control surface stiffness; half chord distance b; dimensionless distances a, c (from the mid-chord to respectively the elastic axis and the hinge location), and x_α and x_β (from elastic axis to airfoil center of gravity and from hinge location to control surface center of gravity); wing mass per unit span m_s; moment of inertia of the section about the elastic axis I_α; and the moment of inertia of the control surface about the hinge I_β.

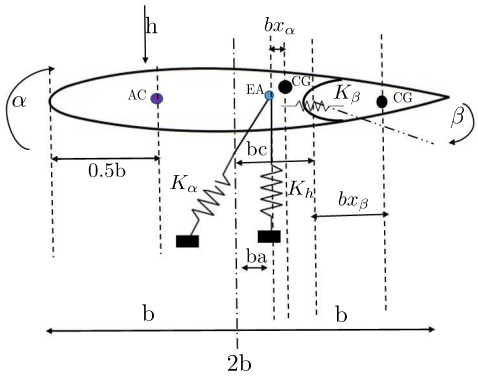

Fig. 2. Airfoil section sketch.

Theodorsen's unsteady formulation is employed to model the aerodynamics [26]. If $X = [h\ \alpha\ \beta]^T$ and $L = [-L_h\ M_\alpha\ M_\beta]^T$ are defined as the vectors of the degrees of freedom and aerodynamic loads respectively, the aerodynamic model provides, in the Laplace domain s, the relation:

$$L(s) = q\big[A_g(\bar{s})\big]X(s) \qquad (7)$$

where the dimensionless variable $\bar{s}$ (=$s\frac{b}{V}$ with V the airspeed) and the dynamic pressure q (=$\frac{1}{2}\rho_\infty V^2$ with ρ_∞ the air density) are introduced. $A_g(\bar{s})$ is called the generalized Aerodynamic Influence Coefficient (AIC) matrix, and is composed of generic terms $A_{g(ij)}$ representing the transfer function from the degree of freedom j in X to the aerodynamic load component i in L. The AIC matrix has a non-rational dependence on the Laplace variable s, thus the final aeroelastic equilibrium is inherently expressed in frequency-domain and is given by:

$$\Big[\big[M_s\big]s^2 + \big[C_s\big]s + \big[K_s\big]\Big]X = q\big[A_g(\bar{s})\big]X \qquad (8)$$

where M_s, C_s and K_s are respectively the structural mass, damping and stiffness matrices. In this work the Minimum State (MS) method [26] is employed to find a rational approximation of $A_g(\bar{s})$, which enables the state-space description of the system to be obtained:

$$\dot{x} = \begin{bmatrix} \dot{x}_s \\ \dot{x}_a \end{bmatrix} = \begin{bmatrix} A_{ss} & A_{sa} \\ A_{as} & A_{aa} \end{bmatrix} \begin{bmatrix} x_s \\ x_a \end{bmatrix} = Ax \tag{9}$$

where A is the state-matrix, x is the vector of states and x_s and x_a are respectively the structural and aerodynamic states, the latter needed for the rational approximation of the unsteady operator. The reason why MS method was selected is that it ensures the lowest size for x_a compared to other approximation algorithms– a desired feature, in terms of state-matrix size, for IQC applications. The interested reader is referred to [27] for further discussions about different aerodynamic approximations and their impact on robust flutter analysis. The total size of the plant n in our example is 9 (6 structural and 3 aerodynamic states). The parameters defining the model are provided in [24], and a detailed definition of the state-matrix A is presented in Appendix A with the aim to allow the reader to reproduce all the results presented in the paper.

It is finally remarked that the system is an open-loop plant, but both the approaches considered in the article can be applied to a closed-loop one, once the state-space description in (9) is opportunely redefined. This could enable the improvements in the nonlinear dynamic response of the system achieved thanks to the adoption of a feedback control law to be estimated in both nominal and uncertain conditions.

1) Linear nominal flutter analysis: Nominal flutter analysis evaluates the largest speed V_f, named flutter speed, below which the dynamic aeroelastic plant is guaranteed to be stable. The stability of the system studied here is related to the spectrum of the state-matrix defined in (9). The nonlinearity, which will be examined later in Section III-C, affects the diagonal term K_β of the stiffness matrix corresponding to the control surface rotation. If this term is taken equal to K_β^L (the linear control surface stiffness, i.e. with no freeplay) and all the other parameters hold their nominal values, a linear nominal analysis of the system can be performed.

In Fig. 3 the eigenvalues corresponding to the structural modes of the system as the airspeed increases from 1 $\frac{m}{s}$ (square marker) to 30 $\frac{m}{s}$ are depicted. The system exhibits flutter at V_f = 24 $\frac{m}{s}$ and ω_f = 38 $\frac{rad}{s}$ (pure imaginary eigenvalue highlighted with the circle marker) with the plunge mode going unstable.

2) Relevance to high-fidelity aeroelastic models: This Section has presented the aeroelastic model employed for the analyses in the rest of the article. Equation (8) is prototypical of current industrial state-of-practice models used for linear flutter analysis, where the structural matrices M_s, C_s, and K_s are usually provided by Finite Element Method (FEM) codes and the AIC matrix A_g is obtained by means of a panel method solver. This motivates the adoption of the typical section to showcase the application of the methodologies presented in this article to the nonlinear flutter problem (see [10], [27] for a more detailed discussion on these aspects).

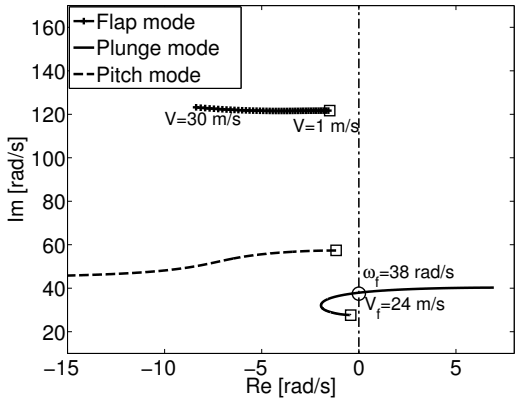

Fig. 3. Linear nominal analysis: poles location as a function of airspeed.

However, when employing them for real aircraft applications, it is expected that practical issues would arise in the LFT modeling phase. Among these, the increase in the size of the problem can be identified as one of the most compelling. A solution consists in applying a modal decomposition to the original large-scale equations and considering only the reduced set for modeling and analysis. Typically for aircraft flutter predictions only the first 5-6 modes are retained as significant for the instability mechanism [8]. A more sophisticated two-step procedure, consisting in firstly reducing the reference models with advanced methods and then building the LFT model by means of polynomial interpolation, was discussed in [28] and is particularly suited for the control system design and analysis applications.

In this regard a strong point of the two approaches presented here is that they pivot on LFT models. This enables powerful techniques available within this framework [2], [16] to address the modeling of complex systems to be exploited. In addition, methods to derive LFT models of nonlinear systems have been recently proposed [29] (also specifically for aerospace applications [30]) and can be used for the present purpose.

B. Model uncertainties

Parametric uncertainties are used to describe parameters whose values are not known with a satisfactory level of confidence. Considering a generic uncertain parameter d, with λ_d indicating the uncertainty level with respect to a nominal value d_0, a general uncertainty representation is given by:

$$d = d_0 + \lambda_d \delta_d \tag{10}$$

where $\|\delta_d\| \leq 1$. This study will take into account a 10% uncertainty in the following parameters: K_h, and K_α (bending and torsional stiffness); static moment of the airfoil S_α; I_α, and I_β (airfoil and flap moment of inertia). As explained in Sec. III-C, the control surface stiffness K_β, affected by freeplay nonlinearity uncertainty, will also be handled within the LFT framework.

The LFT paradigm enables the nominal system to be manipulated by simply introducing the expression (10), specialized for each uncertain parameter, into the state-matrix (9) and using well-established realization techniques (e.g. LFR toolbox [16]) to obtain the corresponding upper LFT (1). See [27] for a detailed presentation of LFT modeling applied to aeroelastic

systems. Here it is just remarked that a plant described through its state-space realization and affected by uncertainties can be seen as an LFT with two blocks in the feedback channels: Δ_u containing the uncertain perturbations affecting the state-space matrices, and $\frac{1}{s}I_n$ with n the number of states. The coefficient matrix M, obtained through the process outlined before, is partitioned correspondingly, as depicted in Fig. 4.

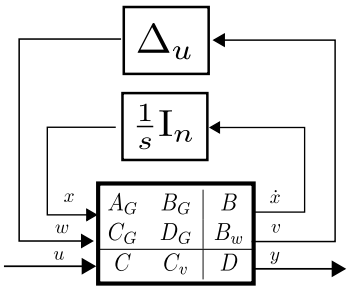

Fig. 4. LFT of an uncertain state-space model.

Particularly relevant, the upper left block of M in Fig. 4 represents the state-space realization of the transfer matrix $M_{11}(s)$ from the signal w to v:

$$M_{11}(s) = C_G(sI_n - A_G)^{-1}B_G + D_G \tag{11}$$

where A_G = A from (9). The subscript G is to remark that M_{11} coincides with the plant G in Fig. 1. This mathematical representation of the uncertain plant is the starting point for the study of the robust stability of the system with either μ or IQC analysis.

μ analysis can be straightforwardly applied to evaluate the robustness of the system. Once the LFT is built up, calculating the matrix M_{11} in (2) basically amounts to evaluating (11) at s = $j\omega$, where ω belongs to the set of discrete frequencies employed in the analyses. The Robust Control Toolbox (RCT) in MATLAB [4] will be adopted in this work. The calculation (2) can then be performed (e.g. with the routine *mussv*) simply providing M_{11} and specifying the real or complex nature of the uncertainties (in this study always real) and their repetitions.

IQC analysis requires to characterize Δ_u in terms of a multiplier Π satisfying (4). It is well-known that for the case of constant real scalar uncertainties a candidate is:

$$\Pi^R = \begin{bmatrix} X(j\omega) & Y(j\omega) \\ Y(j\omega)^* & -X(j\omega) \end{bmatrix} \tag{12}$$

where $X(j\omega)$ = $X(j\omega)^* \geq 0$ and $Y(j\omega)$ = $-Y(j\omega)^*$ are generic bounded and measurable matrix functions (named D-G scalings in robust control theory) [1]. The multiplier in (12) is usually parameterized assuming as basis functions of Ψ combinations of first order low-pass filters. The IQCβ toolbox allows the problem to be formulated by declaring the connections among the signals of the system by *linking* them through appropriate sub-functions. Recalling the feedback interconnection in Fig. 1 (with $r = f = 0$), the relation from w to v is given by state-space realization in (11). The relation from v to w can instead be defined by means of the sub-function `iqc_ltigain`, which implements the parametrization of the multiplier (12), once the poles a_f of the filters are chosen (this will be detailed in Section V). In the end, G and Ψ are defined by means of their state-space realizations, the former provided by the analyst through LFT modeling and the latter directly implemented in the IQC solver, thus the LMI problem in (6) can be solved.

This Section has considered the formulation of the linear robust stability problem when μ analysis and IQC are employed. It is a known fact [1], [17] that the RS calculation build in both cases on the same theoretical premise. However, an important difference is that thanks to the KYP lemma the LMI test in (6) does not rely on a discretization of the frequency range, which for numerical reasons is usually done in μ implementation [4] (i.e. recall the gridding needed to evaluate M_{11}). A worth mentioning exception to this common practice in s.s.v. analysis is represented by a recently developed μ library [31] which guarantees the maximum value of μ_{UB} and μ_{LB} over a *continuum* range of frequencies.
In conclusion, the stability certificate obtained with IQC is granted on the whole frequency spectrum. However, this valuable property is penalized by the need to parameterize Π with a finite basis of rational functions and hence the feasibility of the LMI problem is only a sufficient condition on the stability of the system (i.e. nothing can be said if the test fails). These considerations motivate some of the analyses performed in Section V and will be reflected in the results shown therein.

C. Freeplay nonlinearity

Freeplay, also called dead-zone or threshold, often arises in mechanical and electrical systems where the first part of the input is needed to overcome an initial opposition at the output, as schematically depicted in Fig. 5. The freeplay nonlinearity for the system is concentrated in the control surface stiffness K_β. The mathematical expression for the elastic moment M_β^E can be written as:

$$M_\beta^E = \begin{cases} K_\beta^L(\beta - \bar{\delta}); & |\beta| > \bar{\delta} \\ 0; & |\beta| < \bar{\delta} \end{cases} \tag{13}$$

where $\bar{\delta}$ is defined as the (positive) freeplay size and K_β^L is the flap stiffness in the linear case ($\bar{\delta}$=0). It is worth noting some important properties of this nonlinearity, which will be later exploited: it is odd (i.e. the relation is symmetric about the origin), memoryless (i.e. only one output is possible for any given value of the input), and static (i.e. no dependence upon the input derivatives). In order to recast the problem in the framework of Fig. 1 via LFT, the control surface stiffness K_β is handled as discussed in Section III-B for uncertain parameters (see details later).

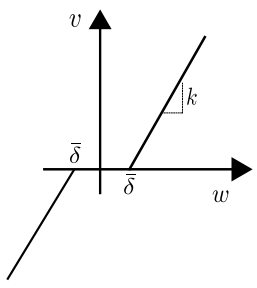

Fig. 5. Freeplay nonlinearity.

1) Description via DF: The DF function N^F associated with freeplay can be obtained analytically [5] through Fourier integrals applying the definition in (3):

$$\begin{cases} 0; & \beta_s < \bar{\delta} \\ \frac{k}{\pi}\left[\pi - 2\sin^{-1}(\frac{\bar{\delta}}{\beta_s}) - 2(\frac{\bar{\delta}}{\beta_s})\sqrt{1-(\frac{\bar{\delta}}{\beta_s})^2}\right]; & \beta_s > \bar{\delta} \end{cases} \tag{14}$$

where β_s is the amplitude of the sinusoidal motion of the control surface. Due to the aforementioned properties held by this nonlinearity, its describing function is a pure real gain (i.e. θ = 0) not depending on frequency, but only on the amplitude of the input signal B (here specified as β_s), in particular on its ratio with $\bar{\delta}$.

The application of DF enables an expression for the elastic moment M_β^E in (13) to be given:

$$\begin{aligned} M_\beta^E &= K_\beta^{QL}\beta \\ K_\beta^{QL} &= N^F(\beta_s)K_\beta^L \end{aligned} \tag{15}$$

where K_β^{QL} is the quasi-linear flap stiffness and N^F is taken from (14) with $k = 1$ (note that $0 < N^F < 1$). In other words, the nonlinear flap stiffness K_β is replaced by the quasi-linear stiffness $K_\beta^{QL}(\beta_s)$, which is a function of the flap rotation amplitude β_s. The flutter speed V_f, obtained from an eigenvalue problem equivalent to the one in Fig. 3 but with K_β = K_β^{QL}, is thus associated with an LCO of amplitude β_s and frequency ω_s equal to the imaginary part of the unstable eigenvalue. As mentioned early, the knowledge of *amplitude* and *frequency* of the nonlinear oscillations is instrumental in order to assess if the constraints prescribed on the airframe's accelerations are met.

2) Description via IQC: If IQC analysis is pursued, a characterization of Δ, here coinciding with the nonlinear operator ϕ (i.e. $w(t)$ = $\Delta(v(t))$ = $\phi(v(t),t)$)), is required. In order to reduce the conservatism of the analyses, a set of multipliers, reflecting different properties of the nonlinearity, is adopted. For example, freeplay can be generically defined as a memoryless sector nonlinearity with bounds [α, η]:

$$\alpha v^2 \leq \phi(v(t),t)v \leq \eta v^2 \quad \forall v \in \mathbb{R}, t \geq 0 \tag{16}$$

The associated multiplier Π^S is:

$$\Pi^S = \begin{bmatrix} -2\alpha\eta & \alpha+\eta \\ \alpha+\eta & -2 \end{bmatrix} \tag{17}$$

In the IQCβ toolbox this multiplier can be assigned to the nonlinear channel of the system by invoking the sub-function `iqc_sector`. Since this is a static IQC, no parametrization is required and the only options to be specified are the sector bounds. A *global* description of the relation in (13) is obtained specifying $\alpha = 0$ and $\eta = K_\beta^L$. Section V will investigate and motivate possible alternative definitions of the sector bound.

In order to capture the time invariance of the freeplay, the Popov multiplier can be used:

$$\Pi^P = \Lambda \begin{bmatrix} 0 & j\omega \\ -j\omega & 0 \end{bmatrix} \tag{18}$$

where Λ is a decision variables. Due to the unboundedness of Π^P on the imaginary axis, a loop transformation $\Delta_1 = \Delta \circ \frac{1}{s+1}$ is typically employed (due to this, Π^P can be employed only if the plant G is strictly proper). This multiplier can be assigned with the sub-function `iqc_popov_vect` and, since it does not require any dynamic parametrization, it is defined simply by specifying the sign of Λ (in this work left unconstrained).

A further refinement of the IQC description can be obtained observing that the freeplay is a monotonic and odd function, and thus a slope restriction in the sector [α_1, η_1] holds. These properties lead to the Zames-Falb IQC [1] (here reported for $\alpha_1 = 0$ and $\eta_1 = 1$):

$$\Pi^{ZF} = \begin{bmatrix} 0 & 1+H(j\omega) \\ 1+H(j\omega)^* & -2-2\,\mathrm{Re}(H(j\omega)) \end{bmatrix} \tag{19}$$

where $H \in \mathbb{RL}_\infty$ is arbitrary except that the $\mathcal{L}_1$-norm of its impulse response must be smaller than one. This multiplier can be selected in IQCβ with the sub-function `iqc_slope_odd`, which requires, other than the sector bounds, also the length N_H and the pole location a_H of the expansion that defines H:

$$H(s) \backsimeq \sum_{k=0}^{N_H} \frac{x_k}{(s+a_H)^{k+1}} \tag{20}$$

where x_k are the associated decision variables. More than one pole can be imposed by invoking i times `iqc_slope_odd` and specifying N_{H_i} and a_{H_i}.

To conclude the IQC description of freeplay, it is proposed here to compute the plant G by building an LFT of the nonlinear stiffness K_β, that is, treating it as if it was an uncertain parameter. Once the sector bound [α, η] is specified, a range of variation $K_{\beta-1} < K_\beta < K_{\beta-2}$ is defined, with $K_{\beta-1} = 2\alpha - \eta$ and $K_{\beta-2} = \eta$. In this way, after the range normalization $\|\delta_{K_\beta}\| \leq 1$, the sector [0,1] automatically holds for Π^S (note that with such a definition $K_\beta = \alpha$ when $\delta_{K_\beta} = 0$ and $K_\beta = \eta$ when $\delta_{K_\beta} = 1$). With this implementation, the nonlinear uncertain system can be manipulated efficiently within a unified framework.

D. LFT models

As stressed in Sections III-B and III-C, both the approaches rely on descriptions of the plant G formulated as LFTs. The operator Δ will gather the uncertain parameters Δ_u and/or the control surface freeplay ϕ depending on the considered problem. Table I gives a recapitulation of the three LFTs adopted in this work in terms of included parameters and total dimension of Δ.

TABLE I
LFT MODELS EMPLOYED

	Parameters $\in \Delta$	Δ size
LFT 1	K_β	1
LFT 2	K_h, K_α, S_α, I_α, I_β	7
LFT 3	K_h, K_α, S_α, I_α, I_β, K_β	8

LFT 1 represents a nonlinear nominal problem, since only the freeplay is included (Δ = ϕ); LFT 2 describes a linear robust problem with stiffness and mass uncertain parameters (Δ = Δ_u); LFT 3 consider the nonlinear robust problem featured by structural uncertainties and nonlinearity (Δ = diag(Δ_u,ϕ)).

IV. Quasilinear robust analysis with DF

This Section shows the results obtained from the application of the DF-μ approach to the study of LCOs in the wing section affected by freeplay and uncertainties.

After a fundamental harmonic solution for the flap rotation $\beta = \beta_s \sin(\omega t)$ is assumed, the corresponding value of N^F (and K_β^{QL}) fixes the term associated with ϕ in the Δ block of the considered LFT. If no uncertainties are included in the model (as in LFT 1), the flutter properties in terms of speed and frequency can be directly obtained through an eigenvalue analysis (as shown in Section III-A for the linear case). Fig. 6 showcases the values of flutter speed V_f and associated frequency ω_s corresponding to a variation of flap stiffness between 0 and the linear value K_β^L (that is, as the associated describing function N^F varies from 0 and 1). The results are in good agreement with others from the literature [23], [24] (the latter reference provides also experimental results).

An interesting feature detectable in Fig. 6 is the existence, depending on the value of K_β^{QL}, of a low (LF) and high (HF) flutter frequency (dashed line) associated with the instability. The physical reason for this is that two distinct modes, respectively the plunge and pitch one, go unstable (i.e. are associated with the smallest unstable speed V_f) as K_β^{QL} varies.

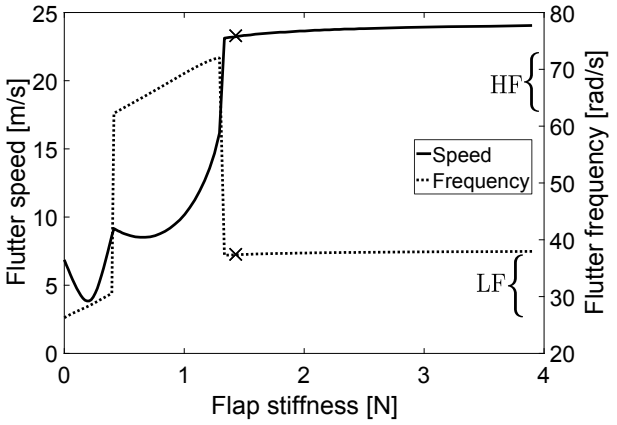

Fig. 6. Flutter speed and frequency vs. flap stiffness for LFT 1.

Due to the existing relation between K_β^{QL} and β_s (15), these results can be shown in a plot airspeed vs. oscillation amplitude, see Fig. 7. This figure serves to emphasize the LCO phenomenon. The DF method is instrumental in guaranteeing this connection and enabling to transfer the information coming from multiple linear flutter analyses to an LCO characterization. For the interested reader, this aspect is further addressed in [32]. Stable and unstable oscillations are depicted respectively with solid and dashed lines, according to the criterion in [33]. It is worth stressing that the latter are not physically meaningful because they represent a dynamic response not occurring in reality (the system will exhibit only the stable LCO branches).

Four regions can be identified in Fig. 7 as the airspeed increases: (i) $V<V_0(=3.8\frac{m}{s})$, where the system is stable; (ii) $V_0<V<V_1(=9\frac{m}{s})$, where the system undergoes LCOs associated with the plunge instability (with amplitude given by the upper stable branch); (iii) $V_1<V<V_2(=23.2\frac{m}{s})$ where the LCO switches to the pitch instability (the frequency correspondingly changes, as in Fig. 6) and the amplitude visibly increases; and (iv), for speeds greater than V_2 where there is an asymptote in the LCO amplitude corresponding to a sizable growth of the airfoil oscillations.

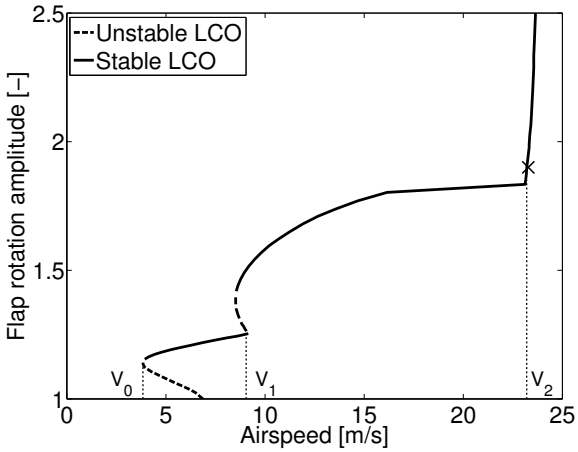

Fig. 7. Flap rotation LCO amplitude $\frac{\beta_s}{\delta}$ against airspeed for LFT 1.

If the nonlinear system is also affected by uncertainties (LFT 3), it is of interest to describe how the stability properties (in terms of V_0), and the LCO features (represented by amplitude β_s, frequency ω_s and the other characteristic speeds) vary due to the terms in Δ_u. This task can be approached as follows: for a given amplitude β_s, the block ϕ has a fixed value and the associated LFT 2 can be evaluated; the problem can then be formulated as a standard RS calculation with μ, looking at the smallest airspeed at which the system is robustly unstable (i.e. $\mu = 1$) and at the related peak frequency. As a first illustrative example, Fig. 8 shows the s.s.v. of the LFT 2 obtained for $K_\beta^{QL} = 1.43$ N (N^F=0.367, $\frac{\beta_s}{\delta} = 1.9$). The nominal flutter - (LCO) properties of this plant are highlighted in Figs. 6 - (7) with a cross marker. This analysis thus enables the effect of the parametric uncertainties on the LCO taking place in nominal conditions at an airspeed V_f = $23.2\frac{m}{s}$ and a frequency $\omega_s = 37\frac{rad}{s}$ to be described.

Upper and lower bounds are reported for completeness in the plot, featuring two distinct peaks. The smaller one takes place at a low frequency (close to the one of the nominal case), whereas the peak μ_{UB} = 1 has a higher frequency of approximately $80\frac{rad}{s}$. The upper bound analysis suggests that the LCO associated with the amplitude of $\frac{\beta_s}{\delta} = 1.9$ drastically changes with respect to the nominal case in that it takes place at a considerably smaller airspeed (V = 10.3 $\frac{m}{s}$) and at a different frequency (pointing at a different mode prompting the nonlinear response). Although no definitive conclusions can be drawn from Fig. 8, due to the gap in the bounds around the highest peak, this result suggests the need for further investigations.

Adding to the issue of the mismatch in bounds, a conclusive analysis should take into account the whole range of quasilinear stiffness K_β^{QL} in order to depict what is named here as the *worst-case LCO curve*, i.e. the equivalent of Fig. 7 where a measure of the LCO properties degradation in the face of the uncertainties is provided. To this end, a flap

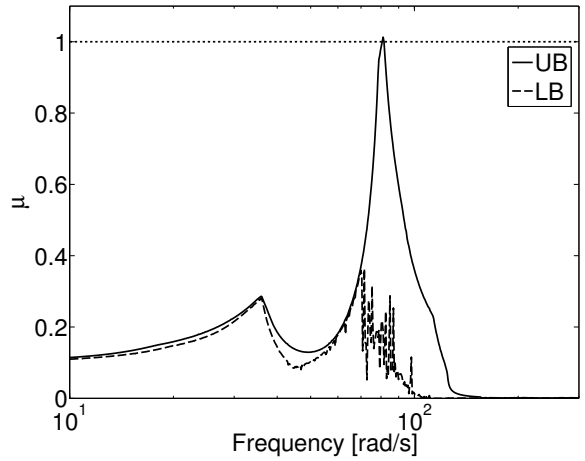

Fig. 8. μ analysis of LFT 2 at V = 10.3 $\frac{m}{s}$ and K_β^{QL} = 1.43 N.

stiffness gridding is calculated and, at each point, a bisection-like algorithm searching for the airspeed V which attains first the RS violation condition (as in Fig. 8) is implemented. In particular, two curves are presented: one for the condition $\mu_{UB} = 1$ and one for $\mu_{LB} = 1$. The results are shown in Fig. 9, which depicts the two corresponding LCO curves as well as the nominal for comparison purposes.

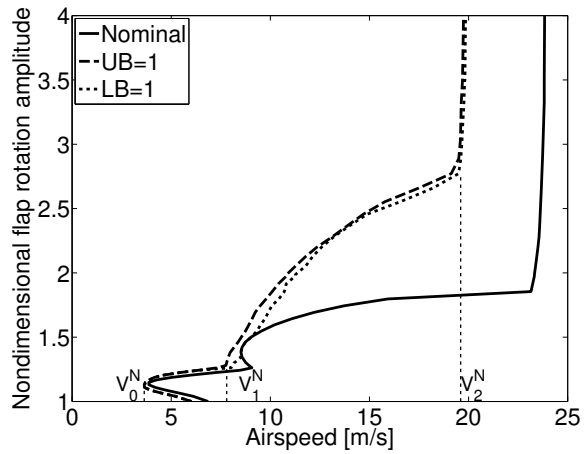

Fig. 9. LCO amplitude $\frac{\beta_s}{\delta}$ against airspeed– the worst-case LCO curve.

This plot can be interpreted as a worst-case analysis of the nonlinear flutter problem in terms of LCO onset and amplitude. In fact, it assesses how the properties discussed before (with reference to Fig. 7) degrade. The first information that can be inferred is the smallest airspeed for which the system experiences LCO. The assumed set of uncertainties slightly decreases this value from $V_0 = 3.8\frac{m}{s}$ to $V_0^N = 3.6\frac{m}{s}$. As the airspeed is increased, the regions highlighted in Fig. 7 are still detectable but V_1 and V_2 are shifted towards smaller values (V_1^N and V_2^N). Furthermore, the plot also allows a significant deterioration in amplitude in the third region to be clearly appreciated. This trend was somehow foreseen in Fig. 8, but finds here a rigorous confirmation (note that the two dashed curves are very close meaning good agreement between the bounds). Although not reported in the plot, at each LCO point it is also possible to associate the oscillation frequency (corresponding to the peak value of μ). This information can provide physical insights into the problem. In this case, for example, it suggests (recall Fig. 8) that the drastic increase in amplitude (with the gap nominal-robust becoming large) can be ascribed to the high frequency (pitch) LCO which is responsible for shifting towards left the asymptote (vertical branch).

In conclusion, this analysis provides a robust characterization of the stability of the nonlinear system and its post-critical behaviour in terms of both amplitude and frequency which, as motivated, are highly relevant engineering parameters.

V. Nonlinear robust analysis with IQCs

This Section presents the application of IQC analysis to the studied test case. The power of this technique lies in the capability to handle uncertainties and nonlinearities in the same framework. However, it is acknowledged that a possible drawback lies in the conservatism associated with the results. This can be ascribed to various causes, and this work investigates two aspects: the selection of the multipliers and the local/global validity of the results.

A. Sensitivity of results to the multipliers

The first analysis employs LFT 1 and aims to give a stability certificate for the nominal airfoil affected by freeplay. Once the IQC description of the nonlinearity is provided as documented in Sec. III-C2, the airspeed is increased until the LMI problem in (6) becomes unfeasible (the first airspeed for which this happens is referred to as V_{unf}). In these first analyses it is assumed that the nonlinearity is defined in the sector $[0, K_\beta^L]$, i.e. $\alpha = \alpha_1 = 0$ and $\eta = \eta_1 = K_\beta^L$ as shown in Fig. 10.

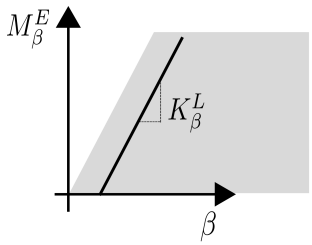

Fig. 10. Sector constraint for stability analyses.

In Tab. II the analyses performed are shown reporting for each test the multiplier (with corresponding options), the size of the LMI problem in terms of decision variables and computation time (performed on a 3.6 GHz desktop PC), and the airspeed V_{unf}.

TABLE II
IQC analysis of LFT 1 (only freeplay)

Multiplier & Options	Size	Time	V_{unf}
Π^S	47	1 s	–
Π^S, Π^P	48	1 s	3.81 $\frac{m}{s}$
Π^S, Π^P,Π^{ZF}([1,1 $\frac{rad}{s}$])	80	1 s	3.82 $\frac{m}{s}$

When only the memoryless sector bounded condition is enforced, no feasible solution is achieved. The Popov multiplier Π^P, encompassing the time invariance of the freeplay, is then

added and this enables to find $V_{unf} = 3.8\frac{m}{s}$, confirmed also via Π^{ZF}. This value is the same as the airspeed V_0 detected in Fig. 7. If the analyses depicted in Figs. 6-7 are recalled, this indicates that the approach of considering the entire sector is equivalent, from a DF perspective, to look for the smallest airspeed such that the system experiences an LCO. The adoption of the entire sector can thus be interpreted as a search for asymptotic stability certificates.
Note also that, due to the good agreement, this analysis may be seen as a (more general) validation of the application of DF to this particular test case (recall the simplifying hypotheses underpinning DF).

The analyses reported in Tab. III investigate the linear robust stability of the LFT 2. In order to draw a parallel with the analyses in Fig. 8 (showing that μ_{UB}=1 at V = 10.3 $\frac{m}{s}$), the same value of K_β is used.

TABLE III
IQC ANALYSIS OF LFT 2 (ONLY UNCERTAINTIES)

Multiplier & Options	Size	Time	V_{unf}
Π^R (1 $\frac{rad}{s}$)	330	9 s	8.6 $\frac{m}{s}$
Π^R (80 $\frac{rad}{s}$)	330	9 s	8.9 $\frac{m}{s}$
Π^R (1 $\frac{rad}{s}$, 80 $\frac{rad}{s}$)	800	70 s	10.3 $\frac{m}{s}$

When only one filter is employed in the multiplier parametrization, the minimum airspeed at which the problem becomes unfeasible (i.e. the aeroelastic system loses its stability) is still lower than what was obtained with μ analysis. However, changing the pole from the default value (i.e. 1 $\frac{rad}{s}$) to one which is closer to the expected flutter frequency (about 80 $\frac{rad}{s}$ from the analyses in Fig. 8) increases the estimation of V_{unf}. The addition of another filter aids to considerably improve the prediction, in particular it yields the same airspeed for which $\mu_{UB} = 1$ in Fig. 8. This results represents an important confirmation of what was shown in Fig. 8, since it holds on the frequency continuum (i.e. not relying as μ generally does on the frequency gridding as it was discussed in Section III-B).

This first set of tests concludes with a nonlinear robust analysis applied to LFT 3, reported in Tab. IV. It is clear from the results that when only one filter is used for Π^R the algorithm is not able to find a feasible solution (regardless of the description provided for Π^{ZF}). In fact, it is decisive to increase the number of filters to 3 in order to match the largest stable airspeed $V_{unf} = 3.6\frac{m}{s}$ found in the analyses of Fig. 9 and therein commented. This IQC description for Π^R is reflected in an increase of the computation burden, but clearly improves the LMI feasibility problem solution.

The results presented in this Section confirm the well-known dependence of IQC predictions on multipliers selection and parametrization. However, in this study the importance of having reference results (here provided by the DF-μ approach, or in general also obtainable with other tools) is stressed. Firstly, they provide a measure of the conservatism associated with the infeasibility of the LMI problem and therefore may point out the need to employ a more refined set of multipliers. While this is typically accomplished with a frequency sweep of the filter poles (time-consuming and not always successful),

TABLE IV
IQC ANALYSIS OF LFT 3 (NONLINEAR ROBUST)

Multiplier & Options	Size	Time	V_{unf}
Π^R (40 $\frac{rad}{s}$) , Π^S,Π^P, Π^{ZF}([1,40$\frac{rad}{s}$])	390	19 s	-
Π^R (80 $\frac{rad}{s}$) , Π^S,Π^P, Π^{ZF}([1,40$\frac{rad}{s}$],[1,80$\frac{rad}{s}$])	450	40 s	-
Π^R (40 $\frac{rad}{s}$, 80 $\frac{rad}{s}$) Π^S,Π^P, Π^{ZF}([1,40$\frac{rad}{s}$])	890	105 s	3.1 $\frac{m}{s}$
Π^R (40 $\frac{rad}{s}$, 80 $\frac{rad}{s}$) , Π^S,Π^P, Π^{ZF}([1,40$\frac{rad}{s}$],[1,80$\frac{rad}{s}$])	980	170 s	3.1 $\frac{m}{s}$
Π^R (1 $\frac{rad}{s}$, 40 $\frac{rad}{s}$, 80 $\frac{rad}{s}$) , Π^S, Π^P, Π^{ZF}([1,40$\frac{rad}{s}$])	1590	530 s	3.6 $\frac{m}{s}$
Π^R (1 $\frac{rad}{s}$, 40 $\frac{rad}{s}$, 80 $\frac{rad}{s}$) , Π^S, Π^P, Π^{ZF}([1,40$\frac{rad}{s}$],[1,80$\frac{rad}{s}$])	1700	790 s	3.6 $\frac{m}{s}$

the availability of auxiliary reference results can also inform the improvement of the parametrization for the multipliers: characterizing the sensitivity of the instability to the blocks Δ_i and therefore focusing only on the refinement of the associated multipliers Π_i; highlighting critical frequencies of the systems. As for the latter aspect, the values of the filter poles are selected here considering the expected unstable frequencies of the systems, obtained by DF-nominal analysis (Fig. 6) or DF-μ approach (Fig. 8), whereas for the former one sensitivity analyses as the ones shown in [32] might also provide invaluable aid.

B. Post-critical analysis with IQC

1) Reduced sector condition: The certificates found with the approach presented so far guarantee asymptotic stability of the system. In fact, only the largest airspeed at which the system settles down to the original equilibrium when subject to any vanishing perturbation can be inferred from the results. This is ascribed to the selection of the standard (*global)* sector for the freeplay nonlinearity (Fig. 10). It is indeed well understood in the literature [1], [17], [19] that results that hold *locally* can enrich the contents of the analyses performed via IQC and reduce their conservatism. This work proposes an alternative definition of the sector condition, aimed at obtaining certificates concerning not only stability properties (as classically done) but also post-critical response features. With this line of reasoning, the sector sketched in Fig. 11 is proposed.

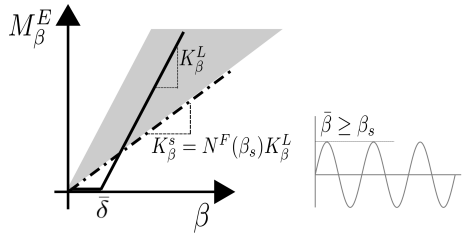

Fig. 11. Local sector constraint for post-critical analyses.

The premise of this relaxation is that the DF method provides, for a given freeplay size $\bar{\delta}$, a relation between the amplitude of the nonlinear response β_s and the equivalent stiffness

associated with the freeplay K_β^{QL} (15). If a lower bound on β_s is assumed, then $K_\beta^{QL}(\beta_s)$ can be taken as the lower limit of the sector K_β^s (dashed-dotted line). The bound on β_s can be interpreted as an oscillation level that can be withstood by the structure, and thus it is tolerated as post-critical response. IQC will then allow for the determination of the largest airspeed V_{unf} such that the system does not experience any oscillatory motion of amplitude greater than β_s. Put it differently, the local characteristic of the analyses prescribes to detect only unstable responses featured by a minimum level of amplitude. In view of the importance of this characterization for the design of aerospace structures (as remarked in the previous sections), this is believed to be a useful tool for nonlinear flutter analysis. Although IQC-based control synthesis is a non-convex problem and thus still an active area of research [34], this description of the freeplay nonlinearity could also be exploited for the design of feedback control laws addressing active reduction of the LCO amplitudes.

2) Results: Table V shows the results obtained applying this approach to LFT 1 and 3. The upper sector limit $\eta = \eta_1$ is fixed at K_β^L as in the previous analyses. A different lower limit for the sector $\alpha = \alpha_1 = K_\beta^s$, with an associated smallest amplitude $\frac{\beta_s}{\bar{\delta}}$, is instead selected for each test and the smallest unfeasible airspeeds (namely V_{unf}^1 for LFT 1 and V_{unf}^3 for LFT 3) are reported. This analysis, repeated on a grid of values of K_β^s, can be interpreted as a nominal and robust characterization of the nonlinear response of the system in that it provides the highest airspeed at which the system can be operated if oscillations below a certain threshold (given by the corresponding $\frac{\beta_s}{\bar{\delta}}$) are tolerated. The parametrization of the multipliers, analyzed and discussed in Sec. V-A, is such so as to provide a reliable IQC description of the problem. It is remarked here that, especially for LFT 3, the multipliers had to be modified with respect to what was reported in the last case of Tab. IV in order to improve the accuracy in the estimation of V_{unf}^3. In fact, a_f in Π^R, as well as N_{H_i} and a_{H_i} in Π^{ZF} proved again to have a tangible influence on the final results and had to be tailored to each single case making use of the heuristic strategy illustrated early. The LMI decision variables were however kept below 2000.

TABLE V
LOCAL IQC ANALYSIS OF LFT 1 AND 3

$K_\beta^s[N]$	$\frac{\beta_s}{\bar{\delta}}$	$V_{unf}^1[\frac{m}{s}]$	$V_{unf}^3[\frac{m}{s}]$
0.01	1.02	3.8	3.6
0.18	1.13	3.8	3.6
0.32	1.21	5.9	4.3
0.86	1.5	9.0	8.45
1.15	1.69	12.2	9.2
1.39	1.9	23.05	10.3
1.72	2.2	23.5	12.3
2.00	2.5	23.6	15.7

Looking at Tab. V it can be seen that the first two values of V_{unf}^1 and V_{unf}^3 match with the predictions obtained using the global sector condition, reported in Tabs. II-IV respectively. If Figs. 7-9 are recalled, it can be observed that both the LCO amplitudes $\frac{\beta_s}{\bar{\delta}} = 1.02$ and $\frac{\beta_s}{\bar{\delta}} = 1.13$ are smaller than the one associated with the smallest LCO speed V_0 (or V_0^N for the LFT 3) in the previous figures– recall that at these airspeeds the system will exhibit an LCO of amplitude $\frac{\beta_s}{\bar{\delta}} \simeq 1.16$). Consistent with the given interpretation of the local sector condition, the analysis returns therefore the corresponding airspeed value (either V_0 or V_0^N). As $\frac{\beta_s}{\bar{\delta}}$ is increased, it becomes evident the advantage of using the sector condition in Fig. 11 since different unfeasible speeds are predicted for each lower sector bound. For $\frac{\beta_s}{\bar{\delta}} \leq 1.5$, the degradation due to the uncertainties, measured by the difference between V_{unf}^1 and V_{unf}^3, is not remarkable. As the amplitude is increased (note that a bold line is employed in Tab. V to emphasize the two regions), it is evident a greater effect of the uncertainties in worsening the response. For example, assume a nominal analysis cleared the system to operate at $V{=}16\frac{m}{s}$ (because it was able to withstand an oscillation of amplitude $1.9\bar{\delta}$). The latter amplitude corresponds to a $K_\beta^s{=}1.39N$ in Tab. V and takes place at $V_{unf}^1{=}23.05\frac{m}{s}$. The proposed analysis then reveals that in the face of uncertainties the system could exhibit an LCO greater than $2.5\bar{\delta}$ (last row of Tab. V) at $V_{unf}^3 = 15.7\frac{m}{s}$, which is actually slightly less than the cleared nominal airspeed- with the risks this represents.

The trend in Tab. V is in good agreement both qualitatively and quantitatively with the worst-case LCO curve in Fig. 9. The intersections of horizontal lines (drawn for different values of the ordinate $\frac{\beta_s}{\bar{\delta}}$) with the nominal and robust curves give points having as x coordinate approximately the corresponding values of V_{unf}^1 and V_{unf}^3. Two curves were provided for the uncertain system, one for $\mu_{UB} = 1$ and another for $\mu_{LB} = 1$. The values of V_{unf}^3 are typically closer to the intersections with the curve $\mu_{UB} = 1$, which is expected since they both give only a sufficient condition for the stability violation. However, the two curves are very close as stressed before.

Finally, note that, for a given value of $\frac{\beta_s}{\bar{\delta}}$, the LCO amplitude β_s experienced by the system is a function of the freeplay size $\bar{\delta}$. Thus this methodology provides, as physically intuitively as possible, an outcome which depends also on this parameter. On the contrary, by looking at Fig. 10, it is apparent that the freeplay size $\bar{\delta}$ has no role in the IQC definition, and therefore will not influence the outcome of the analyses, when the standard approach is employed.

VI. VALIDATION

This Section aims at providing a preliminary validation of the results showcased in Sec. IV-V.

The predictions obtained with the DF approach pivots on the applicability of the filter hypothesis. This is thoroughly addressed for the (nominal) test case in [25], where the Harmonic Balance, a refinement of DF method retaining also higher harmonics than the fundamental one, is employed. Two cases are studied, with respectively 1 harmonic, leading to equivalent results to the DF method, and 3 harmonics. When only the first harmonic is considered, some discrepancy in the predicted amplitude of the LCO branch in Fig. 7 corresponding to the low frequency instability is detected, as opposed to the case with 3 harmonics which almost perfectly match the results obtained through nonlinear time-marching.

In [23] experimental tests are carried out, which confirm the good qualitative agreement with DF and time-marching simulations, although it registers differences even with the latter in the aforementioned speed range. These are ascribed to more complex nonlinear responses exhibiting features such as quasiperiodicity and chaos. Refined time-integration techniques [35], tailored for the simulation of piecewise linear systems, proves to overcome some of these issues and are able to better capture the behaviour shown in the experiments. In this article the validation is pursued by means of time-domain simulations of the nonlinear system, which in contrast to the aforementioned studies, is also subject to uncertainties. The tool presented in [36], allowing to simulate LFR objects [16] in Simulink©, is employed.

In Fig. 12 a comparison, based on the normalized oscillation amplitude $\frac{\beta_s}{\delta}$, between the results given by the two proposed approaches and the nonlinear simulations is presented. As for the former, in view of the good agreement discussed in Sec. V between the two set of results, only the ones from the DF-μ_{UB} are reported (recall Fig. 9) for the case with uncertainties. This is compared with the worst-case predictions obtained via a Monte Carlo/vertex approach, where all the possible combinations of the extreme values of the 5 uncertain parameters are simulated, and the largest amplitude of oscillation is reported. The 32 tested cases are deemed to provide a sufficiently good estimation of the worst-case amplitude because the uncertainty set is a polytope [2].

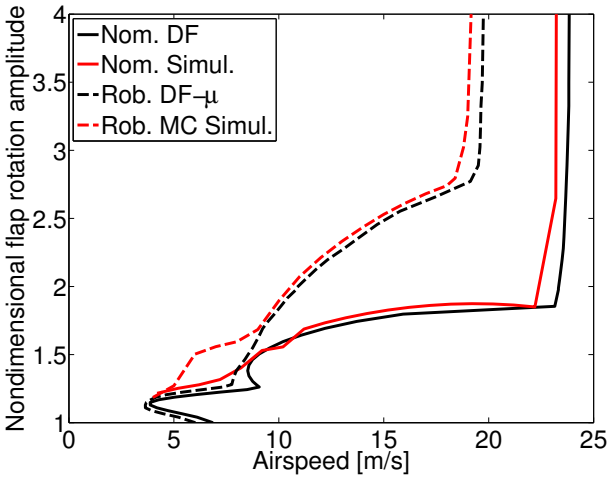

Fig. 12. LCO amplitude $\frac{\beta_s}{\delta}$ against airspeed– validation via simulation.

First, the nominal analyses are discussed (i.e. the solid lines in Fig. 12). It is apparent a good agreement in terms of smallest LCO speed V_0 and amplitudes, featuring a mismatch of less than 5 %, except in a limited airspeed range, the same detected in [23], where the response is nonperiodic.

When the scenario with uncertainties is considered, it is noted that all the conclusions drawn in the previous sections are confirmed: little effect on V_0; sizeable growth in amplitude for $V>V_1$; drastic decrease in the asymptote speed V_2. The predictions are in good agreement also quantitatively, except for the branch in the speed range $5.5\frac{m}{s}<V<9\frac{m}{s}$.

To better interpret these results, the worst-case (i.e. featuring the maximum amplitude) time-domain responses at two different speeds are considered. The plot in Fig. 13 shows the behaviour of the system at $V=6\frac{m}{s}$ for different initial conditions (all the states are set to zero except β, whose initial value is reported in the legend). The main features apparent from the plots are nonperiodicity and sensitivity to the initial conditions, hinting at a chaotic behaviour of the system in this range, which was also found in [23] for the nominal case. It is thus inferred here that adverse combinations of the uncertainties are able to exacerbate this feature of the system, which cannot be accurately captured with the approaches proposed in the present work. In fact, the accuracy of the nonlinear simulations itself is not ascertained in these conditions when standard time-marching algorithms are employed [35].

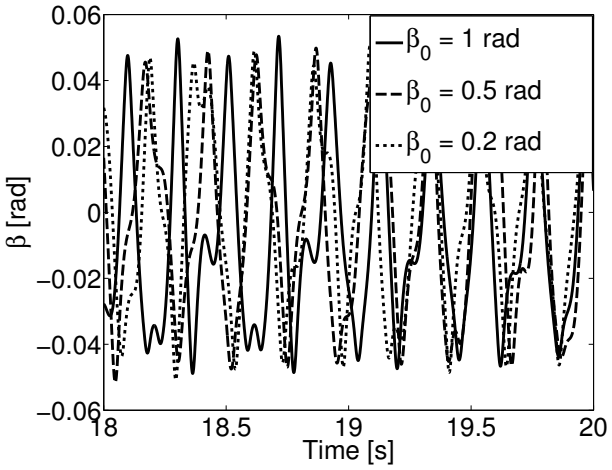

Fig. 13. Worst-case response at $V = 6\frac{m}{s}$ for different initial conditions.

Fig. 14 shows the case at $V = 10.3\frac{m}{s}$, where a Limit Cycle can be clearly detected. It has an amplitude β_s=0.074 rad (i.e. $\frac{\beta_s}{\delta}$=2) and a period $T = 0.077s$. This is in good agreement with the analyses in Fig. 8, where the worst-case detected by μ featured a frequency of approximately $80\frac{rad}{s}$ and a value of K_β^{QL} = 1.43 N which corresponds, using the relations in (15) and (14), to $\frac{\beta_s}{\delta}$=1.9.

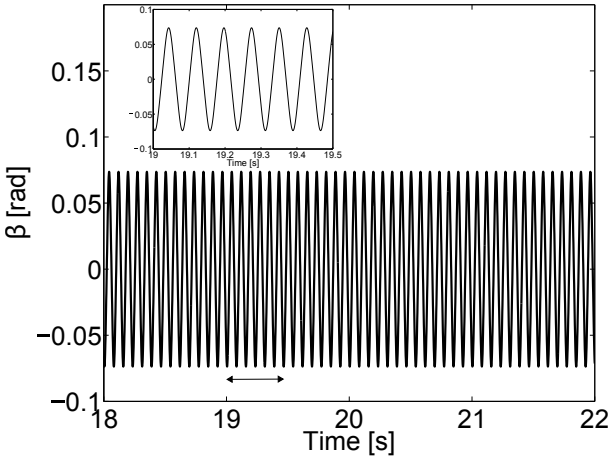

Fig. 14. Worst-case response at $V = 10.3\frac{m}{s}$.

This Section is concluded with a brief discussion upon the applicability of the approaches presented in this work. Based

on the validation campaign performed, it can be affirmed that when the hypotheses underlying DF theory (mentioned in Sec. II-B and further commented in [5], [32]) to the particular system examined are fulfilled, the DF method leads to accurate quantitative predictions of the LCO phenomenon, and its use in conjunction with μ can give important indications on the effect of the uncertainties. IQC, on the other hand, can guarantee the absolute stability of the system without the same assumptions on the nature of the signal. However, when this is used to study the post-critical behaviour of the system as proposed in this article, its accuracy is inherently linked to the DF applicability. This is a consequence of the definition of the restricted sector condition in Fig. 11, which uses N^F to formulate a lower bound on the sector. However, the core idea presented here of redefining the IQC multipliers based on *some* features of the system nonlinear response can in principle inspire other solutions which are not affected by this limitation.

VII. Conclusion

This paper focused on the study of stability and post-critical behaviour of an airfoil subject to freeplay and parametric uncertainties. Two approaches were presented, the first featured by a combination of Describing Function and μ analysis, and the second based on Integral Quadratic Constraints. The modeling aspects of each technique with respect to uncertainties and nonlinearities were detailed in order to stress the known connections and new interpretations. When the DF-μ approach was adopted, the conditions at which the system lost stability could be determined, and changes in the nonlinear response with respect to the nominal case, estimated. In particular, it was proposed a representation of the results through a worst-case LCO curve depicting the worst-case degradation in the response of the system (in terms of oscillation amplitude) due to the uncertainties.

In showcasing the results obtained with the IQC approach, emphasis was put on the conservatism of the analyses. In a first step, this was ascribed to the selection and parametrization of the multipliers and a sensitivity study of the results was performed, proving convergence to the ones obtained with the first approach. Then, a strategy allowing IQC to study the post-critical response of the plant was proposed, based on a restricted sector bound condition aimed at detecting only nonlinear responses featuring a minimum level of amplitude. The results obtained with this description, believed to have practical consequences for analysis and potentially also control synthesis, were compared with the outcomes of the DF-μ approach, showing a very good agreement.
Finally, a validation of the proposed frameworks, based on nonlinear time-marching simulations, was performed. This suggests that both the approaches are able to cope with the nonlinear uncertain problem examined in the article. Qualitative trends are well captured, and quantitative estimations are reliable except in limited cases when the hypotheses underpinning the approaches are violated.

Appendix A
Airfoil model

The state-matrix A in (9) can be written as:

$$A = \begin{bmatrix} 0 & I & 0 \\ -\bar{M}^{-1}\bar{K} & -\bar{M}^{-1}\bar{C} & -\bar{M}^{-1}D \\ 0 & E & R \end{bmatrix} \tag{21}$$

with $\bar{M} = M_s - \frac{1}{2}\rho_\infty b^2 A_2$, $\bar{C} = C_s - \frac{1}{2}\rho_\infty b V A_1$, and $\bar{K} = K_s - \frac{1}{2}\rho_\infty V^2 A_0$. $\bar{M}$, $\bar{C}$ and $\bar{K}$ are respectively the aeroelastic inertial, damping and stiffness matrices [27].
The operators involved in the definition of A are:

$$A_0 = \begin{bmatrix} 0 & -1.5959 & -0.9719 \\ 0 & 0 & -0.0419 \\ 0 & -0.0023 & -0.0038 \end{bmatrix}$$

$$A_1 = \begin{bmatrix} -6.3765 & -1.6061 & -0.3212 \\ -0.0037 & -0.1001 & -0.0328 \\ -0.0093 & -0.0128 & -0.0043 \end{bmatrix}$$

$$A_2 = \begin{bmatrix} -6.254 & -0.3996 & -0.0338 \\ -0.3988 & -0.0394 & -0.0041 \\ -0.0319 & -0.0037 & -0.0006 \end{bmatrix}$$

$$D = \frac{1}{2}\rho_\infty V^2 \begin{bmatrix} 2.9931 & 3.0064 & 3.0642 \\ 0.0029 & -0.0112 & -0.0889 \\ 0.0045 & 0.0035 & -0.0038 \end{bmatrix}$$

$$E = \begin{bmatrix} -0.0948 & 0.1523 & 0.0968 \\ -0.3913 & 0.0281 & 0.0409 \\ 0.0282 & 0.0234 & 0.0093 \end{bmatrix}$$

$$R = \frac{V}{b} \begin{bmatrix} -0.1 & 0 & 0 \\ 0 & -0.4 & 0 \\ 0 & 0 & -0.7 \end{bmatrix}$$

$$M_s = \begin{bmatrix} 3.3843 & S_\alpha & 0.00395 \\ S_\alpha & I_\alpha & I_\beta + 0.000502 \\ 0.00395 & I_\beta + 0.000502 & I_\beta \end{bmatrix}$$

$$C_s = \begin{bmatrix} 2.2223 & 0.0222 & 0.0002 \\ 0.0222 & 0.0208 & 0.0011 \\ 0.0002 & 0.0011 & 0.0008 \end{bmatrix}$$

$$K_s = \begin{bmatrix} K_h & 0 & 0 \\ 0 & K_\alpha & 0 \\ 0 & 0 & K_\beta \end{bmatrix}$$

The dependence of the operators on the airspeed V and on the parameters subject to nonlinearity and uncertainty is left explicit. The corresponding linear/nominal values are given in Tab. VI.

References

[1] A. Megretski and A. Rantzer, "System analysis via integral quadratic constraints," *IEEE Transactions on Automatic Control*, vol. 42, no. 6, pp. 819–830, Jun 1997.

[2] K. Zhou, J. C. Doyle, and K. Glover, *Robust and Optimal Control*. Prentice-Hall, Inc., 1996.

TABLE VI
PARAMETERS OF THE AIRFOIL MODEL

Name	Value	Name	Value
I_α	0.01347 $kg\ m$	I_β	0.0003264 $kg\ m$
S_α	0.08587 kg	K_h	2818.8 $\frac{N}{m^2}$
K_α	37.3 N	K_β^L	3.9 N
b	0.127 m	ρ_∞	1.225 $\frac{kg}{m^3}$
$\bar{\delta}$	2.12°		

[3] C. Desoer and M. Vidyasagar, *Feedback Systems: Input-output Properties*, ser. Classics in Applied Mathematics. Society for Industrial and Applied Mathematics, 1975.

[4] G. Balas, R. Chiang, A. Packard, and M. Safonov, *Robust Control Toolbox*, 2009.

[5] A. Gelb and W. E. Vander Velde, *Multiple-Input Describing Functions and Nonlinear System Design*. McGraw-Hill, 1968.

[6] S. Katebi and M. Katebij, "Combined frequency and time domain technique for the design of compensators for non-linear feedback control systems," *International Journal of Systems Science*, vol. 18, no. 11, pp. 2001–2017, 1987.

[7] G. Ferreres, *A practical approach to robustness analysis with aeronautical applications*. New York: Kluwer Academic, 1999.

[8] W. P. Rodden, *Theoretical and Computational Aeroelasticity*. Crest Publishing, 2011.

[9] P. Bansal and D. Pitt, "Uncertainties in control surface free-play and structural properties and their effect on flutter and LCO." AIAA Scitech Conference, January 2014.

[10] B. Danowsky, P. Thompson, and S. Kukreja, "Nonlinear Analysis of Aeroservoelastic Models with Free Play Using Describing Functions," *Journal of Aircraft*, vol. 50, no. 2, pp. 329–336, 2013.

[11] P. Wiggins, *Introduction to Applied Nonlinear Dynamical Systems and Chaos*. Springer-Verlag New York, 2003.

[12] E. Dowell, J. Edwards, and T. Strganac, "Nonlinear aeroelasticity," *Journal of Aircraft*, vol. Vol. 40, no. 5, 2003.

[13] C. Fielding and P. Flux, "Non-linearities in flight control systems," *The Aeronautical Journal*, vol. 107, no. 1077, pp. 673–686, 2003.

[14] J. Gordon, E. Meyer, and R. Minogue, "Nonlinear Stability Analysis of Control Surface Flutter with Freeplay Effects," *Journal of Aircraft*, vol. 45, no. 6, pp. 1904–1916, 2008.

[15] D. Baldelli, R. Lind, and M. Brenner, "Robust Aeroservoelastic Match-Point Solutions Using Describing Function Method," *Journal of Aircraft*, vol. 42, no. 6, pp. 1597–1605, 2005.

[16] J. Magni, "Linear fractional representation toolbox modelling, order reduction, gain scheduling," DCSD, ONERA, Systems Control and Flight Dynamics Department, Technical Report TR 6/08162, 2004.

[17] J. Veenman, C. W. Scherer, and H. Köroğlu, "Robust stability and performance analysis based on integral quadratic constraints," *European Journal of Control*, vol. 31, pp. 1 – 32, 2016.

[18] J. Carrasco, W. P. Heath, and A. Lanzon, "Equivalence between classes of multipliers for slope-restricted nonlinearities," *Automatica*, vol. 49, no. 6, pp. 1732 – 1740, 2013.

[19] E. Summers and A. Packard, "L2 gain verification for interconnections of locally stable systems using integral quadratic constraints," in *49th IEEE Conference on Decision and Control (CDC)*, 2010.

[20] A. Iannelli, A. Marcos, and M. Lowenberg, "Nonlinear stability and post-critical analysis of an uncertain plant with describing functions and integral quadratic constraints," in *56th IEEE Conference on Decision and Control (CDC)*, 2017.

[21] U. Jonsson, C.-Y. Kao, A. Megretski, and A. Rantzer, *A Guide to IQC β: A MATLAB Toolbox for Robust Stability and Performance Analysis*.

[22] C. L. Pettit, "Uncertainty quantification in aeroelasticity: Recent results and research challenges," *Journal of Aircraft*, vol. 41, no. 5, pp. 1217–1229, 2004.

[23] M. Conner, D. Tang, E. Dowell, and L. Virgin, "Nonlinear Behavior of a Typical Airfoil Section with Control Surface Freeplay. A Numerical and Experimental Study," *Journal of Fluids and Structures*, vol. 11, no. 1, pp. 89 – 109, 1997.

[24] D. Tang, E. Dowell, and L. Virgin, "Limit Cycle Behavior of an Airfoil with a Control Surface," *Journal of Fluids and Structures*, vol. 12, no. 7, pp. 839 – 858, 1998.

[25] Liu, L. and Dowell, E. H., "Harmonic Balance Approach for an Airfoil with a Freeplay Control Surface," *AIAA Journal*, vol. 43, no. 4, pp. 802–815, April 2005.

[26] M. Karpel, "Design for Active and Passive Flutter Suppression and Gust alleviation," Nasa Report 3482, 1981.

[27] A. Iannelli, A. Marcos, and M. Lowenberg, "Aeroelastic modeling and stability analysis: A robust approach to the flutter problem," *International Journal of Robust and Nonlinear Control*, 2017.

[28] C. Poussot-Vassal and C. Roos, "Generation of a reduced-order LPV/LFT model from a set of large-scale MIMO LTI flexible aircraft models," *Control Engineering Practice*, vol. 20, no. 9, pp. 919–930, 2012.

[29] K. Hsu, K. Poolla, and T. L. Vincent, "Identification of structured nonlinear systems," *IEEE Transactions on Automatic Control*, vol. 53, no. 11, pp. 2497–2513, Dec 2008.

[30] D. H. Baldelli, R. Lind, and R. Brenner, "Nonlinear aeroelastic/aeroservoelastic modeling by block-oriented identification," *J. of Guidance, Control and Dynamics*, vol. 28, no. 5, pp. 1056–1064, 2005.

[31] C. Roos, "Systems modeling, analysis and control (SMAC) toolbox: An insight into the robustness analysis library," in *2013 IEEE Conference on Computer Aided Control System Design (CACSD)*, 2013.

[32] A. Iannelli, A. Marcos, and M. Lowenberg, "Limit Cycle Oscillation amplitude tailoring based on Describing Functions and μ Analysis," in *Advances in Aerospace Guidance, Navigation and Control*, 2017.

[33] M. Anderson, "Pilot-induced oscillations involving multiple nonlinearities," *J. of Guidance, Control and Dynamics*, vol. Vol. 21, no. 5, pp. pp. 786–791, 1998.

[34] P. Apkarian and D. Noll, "IQC analysis and synthesis via nonsmooth optimization," *Systems & Control Letters*, vol. 55, no. 12, pp. 971 – 981, 2006.

[35] Chen, P. C. and Sulaeman, E., "Nonlinear response of aeroservoelastic systems using discrete state-space approach," *AIAA Journal*, vol. 41, no. 9, pp. 1658–1666, September 2003.

[36] J. M. Biannic, C. Doll, and J. F. Magni, "SIMULINK-based tools for creating and simulating interconnected LFR objects," in *2006 IEEE Conference on Computer Aided Control System Design*.